

Article

Evaluation of Liquid Atomization and Spray Drift Reduction of Hydraulic Nozzles with Four Spray Adjuvant Solutions

Qi Liu ^{1,2,3}, Changfeng Shan ^{1,2,3}, Haiyan Zhang ⁴, Cancan Song ^{1,2,3} and Yubin Lan ^{1,2,3,5,*}

¹ College of Agricultural Engineering and Food Science, Shandong University of Technology, Zibo 255022, China

² Shandong University of Technology Sub-Center of National Center for International Collaboration Research on Precision Agricultural Aviation Pesticide Spraying Technology, Zibo 255022, China

³ Academy of Ecological Unmanned Farm, Shandong University of Technology, Zibo 255022, China

⁴ College of Information and Electrical Engineering, Shenyang Agricultural University, Shenyang 110866, China

⁵ Department of Biological and Agricultural Engineering, Texas A&M University, College Station, TX 77845, USA

* Correspondence: ylan@sdut.edu.cn; Tel.: +86-20-85281421

Abstract: The droplet size distribution following pesticide application practices can significantly impact droplet drift and non-target organisms (animals and plants). However, the relationship among liquid sheet breakup, drop formation, and droplet drift is an area that has been studied over the past 65 years but is still not fully understood. The objectives of this study were severalfold: to examine the liquid sheet breakup following the use of different adjuvants (sodium dodecyl sulfate, aerosol OT, and silicone at 1%) and their effects on the drift via three commonly used commercial spray nozzles (XR, AIXR, and TXVK). The spray sheet and initial droplet size spectrum for each spray was detected by a particle image velocimetry (PIV) system, and the drift for each treatment was measured in a wind tunnel. The nozzle type and the spray solution were found to significantly affect the liquid sheet breakup characteristics. AIXR produced large droplets, and TXVK with short liquid sheet length produced more small droplets. All adjuvants used in these experiments increased the formation of large droplets upon atomization while simultaneously reducing driftable fines (e.g., drops $<150\ \mu\text{m}$). The drift potential can be reduced by up to 66.1% when switching from a fine spray quality (TXVK) to a coarse spray quality (AIXR). The SDS adjuvant provided the most effective drift reduction for XR and TXVK nozzles showing reduced drift potential by 69.2% and 66.3%, respectively, while the silicone adjuvant showed the largest drift reduction for AIXR of 78.3%. The correlation between the liquid sheet length and $D_{V0.5}$ was positive for XR and TXVK nozzles, and there was a significant positive correlation between $<150\ \mu\text{m}$ and drift potential for all nozzles. This work suggests that the drift can be reduced significantly by changing the nozzle type and adding pesticide adjuvant into spray solution, which provided data support for the drift reduction of plant protection drones.



Citation: Liu, Q.; Shan, C.; Zhang, H.; Song, C.; Lan, Y. Evaluation of Liquid Atomization and Spray Drift Reduction of Hydraulic Nozzles with Four Spray Adjuvant Solutions. *Agriculture* **2023**, *13*, 236. <https://doi.org/10.3390/agriculture13020236>

Academic Editor: Jianli Song

Received: 1 November 2022

Revised: 11 January 2023

Accepted: 12 January 2023

Published: 19 January 2023

Keywords: wind tunnel; droplet drift; PIV system; liquid sheet breakup

1. Introduction

Pesticides play a key role in crop pest control and public health [1]. However, pesticide drift is one of the main ways to increase human exposure [2]. Numerous health-related diseases, including Parkinson's disease and neurotoxin diseases, have been shown to be strongly related to the long-term occupational exposure to pesticides [3,4]. In addition, pesticide drift is also a potential threat to surrounding sensitive crops, fish ponds, and surface water [5]. Developed countries have invested a great deal of effort in research on pesticide safety. Entrusted by the UK government, the Local Environmental Risk Assessment for Pesticides has studied buffer zone setbacks for several years [6]. The U.S. Environmental Protection Agency requires 30 m application exclusion zone when using a sprayer that produces fine or very fine size droplets [7]. The European Food Safety



Copyright: © 2023 by the authors. Licensee MDPI, Basel, Switzerland. This article is an open access article distributed under the terms and conditions of the Creative Commons Attribution (CC BY) license (<https://creativecommons.org/licenses/by/4.0/>).

Authority conducted a risk assessment on human exposure for all operators and workers and then published a guidance document on pesticide exposure assessment for workers, operators, bystanders, and residents [8,9]. The topic of drift control has also begun to attract worldwide attention, including from developing countries.

There are many factors affecting pesticide drift [10]. Many studies have investigated how different application technologies affect pesticide drift. Most important for droplet drift is the droplet size, which has been proved by many scholars [11,12]. Based on the principle of controlling droplet size, modification of the rheological properties of the spray solution and the spray nozzle design are the primary technical solutions to produce larger droplets ($>200\text{ }\mu\text{m}$) [12]. Air induction nozzles operate by mixing air into the droplet to reduce the drift potential compared with standard nozzles by as much as 85% [13]. Surface tension and viscosity of the spray liquid are major drift-determining factors [14]. Weather conditions [15–17], mainly wind speed, have a significant effect on pesticide drift. The subject of drift control generated by aerial spray application, especially fixed-wing aircraft, has been developed over 40 years. A mature AGDISP (agricultural dispersion) model was established [18], in which the user predicted the drift potential by inputting pesticide, aircraft type, weather condition, etc., into the system. In recent years, the computational fluid dynamics simulation method has also been gradually applied to the drift prediction of the unmanned aerial vehicle (UAV) sprayer. Songchao [19] calculated the flow field generated by an N-3 agricultural unmanned helicopter by numerical simulation and concluded that a buffer area of 8–10 m was needed when the crosswind speed varied in the range of 1–3 m/s. Based on FLUENT software, Wang et al. [20] studied the spray system of the heavy-lift FR-200 helicopter and found that the higher the speed of aircraft and the closer the nozzle was to the lower part of the body, the worse the anti-drift performance of droplets.

The spray drift associated with the initial droplet size distribution has been extensively studied. Laser diffraction instrumentations are usually used to estimate the diameters of spray droplets that pass through the laser beam. An emitter, which emits the laser beam, and a receiver, which houses a series of 30 or more concentric photodetection cells, constitute the two main components to most laser diffraction instruments [21]. When some droplets are present in the laser beam, the beam is diffracted at an angle proportional to the diameter of the droplets. However, there are spatial distributions of droplet size on the entire atomizing surface for different nozzles [22]. The droplet size measurement at some characteristic locations on the spray sheet by a laser diffraction instrumentation requires not only high position accuracy but also a large amount of work. It is worth mentioning that the development of the liquid sheet and the subsequent formation of ligaments or droplets determines the details of the initial atomization. All these characteristics are strongly influenced by the nozzle shape and the physical properties of the spray liquid. The initial atomization of droplets, especially the droplet size, is an important factor affecting the drift [23]. Therefore, it is necessary to study the effect of the liquid sheet breakup on droplet size and then drift.

Because of the limited space in the wind tunnel, it is difficult to study the drift of UAV in the wind tunnel. Similar to the drift study of the ground spraying machinery in the wind tunnel [24], researchers applied the measurements of the 6 m buffer zone to the drift reduction of the 20 m buffer zone in the field [6]. This research method is also being used for UAV drift testing. The drift data measured in the wind tunnel are equivalent to the drift evaluation of the field through model transformation. Therefore, based on this research method, the same operating parameters as the field test of UAV spraying were set in this study, including spraying pressure, nozzle types, and adjuvant concentration.

Liquid sheets emanating from the nozzle break up into droplets. The resulting initial droplet size distribution is a necessary input for driving the droplet drift. Currently, some researchers [23,25,26] have studied the liquid sheet breakup of agricultural nozzles in the various conditions, but the liquid sheet breakup and spray drift have not been linked. This paper describes a series of experiments that have been conducted to measure the liquid

sheet breakup characteristics by a particle image velocimetry (PIV) system and spray drift formed from a range of spray nozzles and spray liquids in a wind tunnel.

2. Materials and Methods

This experimental study was conducted at the National Center for International Collaboration Research on Precision Agricultural Aviation Pesticide Spraying Technology (NPAAC) at South China Agricultural University, Guangzhou, China, between 25 December and 10 January, 2021 to 2022.

2.1. Flow Visualization Techniques

The spray supply and the 2D PIV system provided a visual flow device for testing the breakup of the liquid sheet and the initial droplet size distribution. The spray supply system included a tank, booster pump, safety valve, pressure-reducing valve, flow meter, pressure gauge, and nozzle. The spraying pressure was adjusted by a safety valve and a pressure-reducing valve, which achieved an accuracy of flow rate of 1%.

The 2D PIV system (Figure 1b) produced by TSI Incorporated containing a PowerView Plus 4MP-HS CCD camera (model 630091), a Nd: YAG Nano laser, a synchronizer (model 610036), and image analysis software (Insight 4G) was used to measure the characteristics of the spray sheet and droplets close to the nozzle. The camera could capture 2048×2048 pixels and was mounted parallel to the liquid sheet surface. The AF-S VR lens (Nikon, Japan) with fixed aperture of F/22 was used in this test. The laser had two independent green lights operating at a maximum rate of 15 Hz, which emitted lights at 7.5 Hz in this test. The laser's exposure time was 5000 μ s, and the camera exposure time was automatically adjusted according to the laser exposure and the laser pulse interval time. The CCD camera and Insight 4G software were connected by a synchronizer (a crucial part of the frame-straddling technique). The laser emitted a short pulse of light at the end of one camera frame and another at the beginning of the next frame. The time interval between the laser pulses was 30 μ s according to the velocity of the liquid sheet and the calculation limit of the instrument.

The camera's field of view (Figure 1a) and focal length ($f = 0.50$ m) were adjusted so that the entire liquid sheet and the initial state of the droplets could fill the frame. The calibration of the relationship between actual size and pixel count was calibrated using the image of a ruler at the focal point of the lens, which was in the same plane as the liquid sheet. A pixel measuring 28.25 μ m in length was selected following debugging and calibration of the instrument. Fifty image pairs were taken for each treatment to analyze the breakup process of the liquid sheet and calculate the droplet size.

2.2. Spray Drift in Wind Tunnel

The spray drift experiments were conducted in the wind tunnel (Figure 2) with the cross-section size of $2.0 \text{ m} \times 1.1 \text{ m}$ (width \times height), which followed the ISO 22856 standards for the low- and high-speed wind tunnel. The wind tunnel can generate airspeeds of 0–52 m/s with inhomogeneity of cross-section airspeed less than 1% and turbulences below 1%. Artificial turf with a thickness of 5 cm was laid at the bottom of the wind tunnel in order to eliminate the rebound effect of the ground on the droplets. The nozzle fixed in the upwind axial plane of the wind tunnel test section was 50 cm away from the top. The distance between the nozzle and the sampling lines was 50 cm in the vertical direction, which was consistent with the installation method of the nozzle in Nuyttens [16], Zhang [27], and Torrent [28].

The polytetrafluoroethylene (PTFE) line with a diameter of 2 mm was used as a collector for collecting the drift in the horizontal and vertical planes in the wind tunnel following the ISO 22866 [29] methodology. The PTFE lines with a length of 2 m and 10 cm from the bottom of the tunnel were at the distances of 2, 3, 4, 5, 6, 7, 8, 9, and 10 m from the spray nozzle. For the airborne drift, a set of PTFE lines were designed at 0.1, 0.2, 0.3, 0.4, 0.5, and 0.6 m above the wind tunnel floor and 2 m downwind from the nozzle. The

ground was represented at 0.1 m in height since it avoided boundary or edge effects caused by the wind tunnel floor. There was a constant wind speed of 2 m/s in the tunnel. The collector setup was illustrated in Figure 2. The wind tunnel ran for 30 min prior to the test to ensure a stable working airflow. In each spraying, a constant spray pressure of 0.3 MPa was applied for 10 s, and each spraying event was repeated three times. In the drift test, Rhodamine-B as a fluorescent tracer at a concentration of 5 g/L was added to the spray liquid listed.

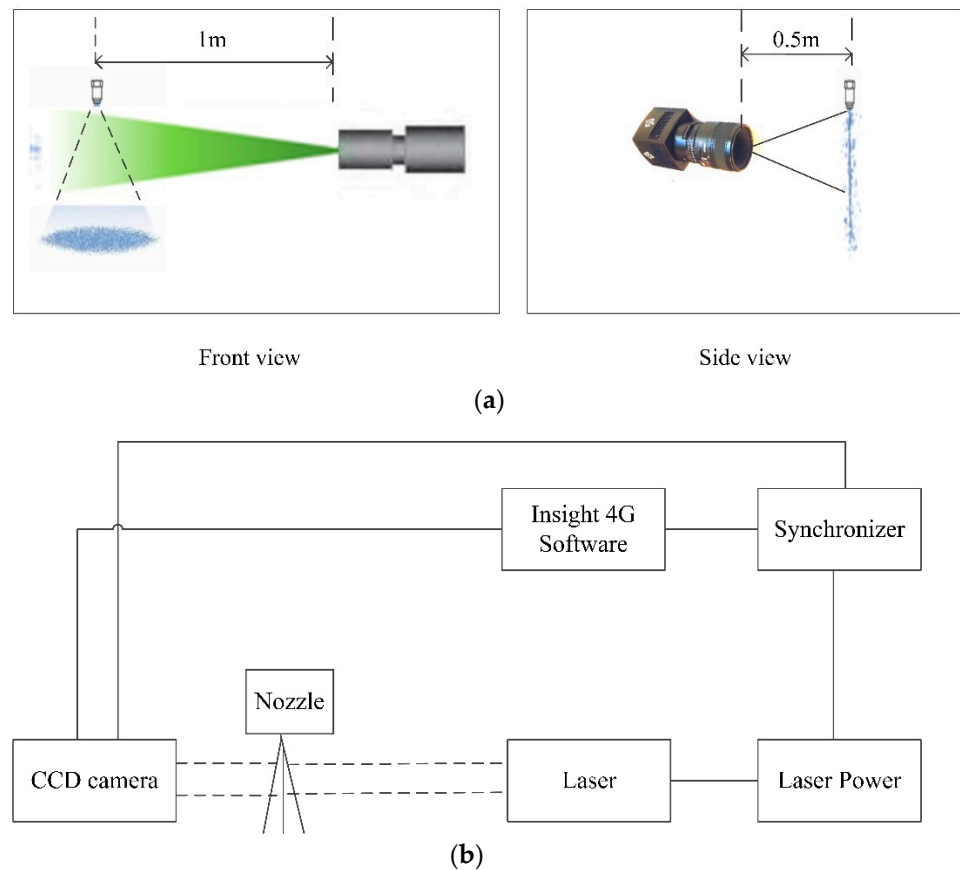


Figure 1. (a) Orientation diagram of the nozzle, laser, and camera. (b) Schematic diagram of the experimental layout for the measurement of liquid sheet breakup.

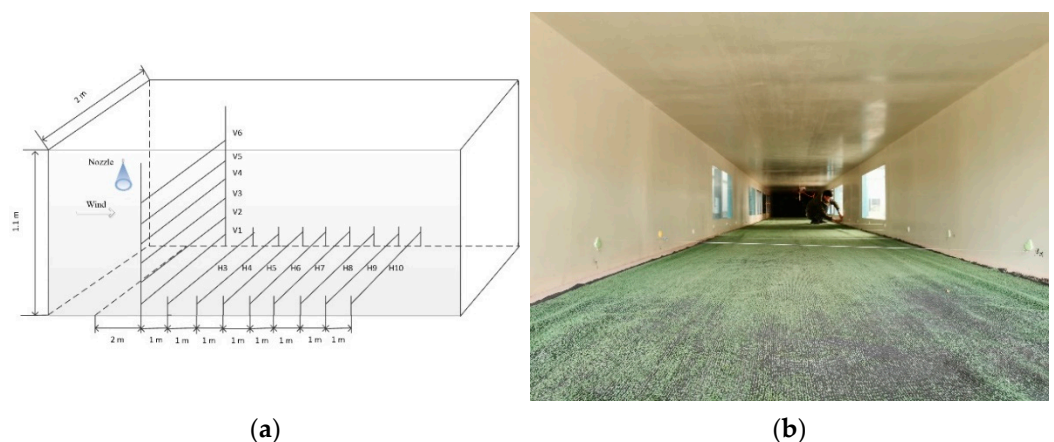


Figure 2. Wind tunnel used in this experiment. (a) Inner dimensions and sampling line layout. (b) Internal structure diagram of physical wind tunnel.

2.3. Sampling Processing

After each drift spray, the wind in the wind tunnel lasted for several minutes until all droplets were deposited in order to reduce test errors and avoid contamination to the subsequent tests. Each PTFE line was put into a sealed bag separately by trained personnel wearing disposable gloves and then was stored in a refrigerator at $-20\text{ }^{\circ}\text{C}$ away from light. According to the deposition on the sampling lines, an appropriate amount of ultrapure water was taken with a pipette gun and was injected into each sealed bag to wash off the tracer on the samplers. After thoroughly rubbing and stirring, part of the eluent was poured into a cuvette for analysis.

Five calibration solutions at the concentrations of 1, 0.5, 0.2, 0.1, and 0.01 mg/L were measured by an F-380 fluorescence spectrophotometer (Tianjin Gangdong Technology Co., Ltd., Tianjin, China). After scanning the spray liquid, the 542 nm excitation wavelength and 579 nm emission wavelength were selected to establish a linear relationship between the fluorescence intensity and the concentration ($Y = 0.002831x - 0.204277$, $R^2 = 99.96\%$). The droplet deposition can be calculated from the fluorometer reading of the test solution, as shown in Formula (1).

$$\beta_{dep} = \frac{(\rho_{smpl} - \rho_{blk}) \times F_{cal} \times V_{dil}}{\rho_{spray} \times A_{col}} \quad (1)$$

where β_{dep} is the drift deposition, μL ; ρ_{smpl} is the fluorimeter reading of each monitored sampler; ρ_{blk} is the fluorimeter reading of the sampler without deposited droplets; F_{cal} is the calibration factor (the relationship between the fluorimeter reading and the tracer concentration); V_{dil} is the volume of dilution liquid used to solute the tracer from the collector, L; ρ_{spray} is the spray concentration of the tracer solute in the spray liquid, g/L; and A_{col} is considered to be 1 as the projected area of the collector for catching the spray drift because the deposition of the entire collector is needed.

2.4. Experimental Conditions

For the measurements of the initial atomization of the liquid sheet and spray drift, the temperature and the relative humidity were kept constant at $25\text{--}27\text{ }^{\circ}\text{C}$ and $50\text{--}60\%$. The nozzles selected for this experiment are listed in Table 1. The spray angle of the AIXR nozzle was smaller than the label angle because the internal structure of the AIXR nozzle was equipped with a pressure drop device to accommodate lower pressure equipment. Three types of nozzles (Teejet Technologies, Glendale Heights, IL, USA) with different liquid sheet breakup mechanisms commonly used by plant protection drones, namely, the Venturi AIXR110015 nozzle, the hollow cone TXVK-4 nozzle, and the fan XR110015 nozzle, were used in this study. In this experiments, the pesticide spray and pesticide extraction procedures would be necessary if an actual pesticide was sprayed. The organic solvents are commonly used to extract pesticide from the sampling medium. Repeated applications of pesticides and the use of organic solvents will result in the large-scale waste disposal, which not only adversely affects laboratory personnel but also harms the environment. Because spray adjuvants are the dominant components that determine the physical properties of pesticide solution, vesicle surfactant sodium bis(2-ethylhexyl) sulfosuccinate [aerosol OT (AOT)] (Shanghai Aladdin Biochemical Technology Co., Ltd., Shanghai, China, CAS Registry Number 577-11-7), sodium dodecyl sulfate (SDS) (neoFroxx GmbH, Einhausen, Germany, CAS Registry Number 151-21-3), and silicone mainly composed of ethoxyl modified trisiloxane (Momentive Performance Materials Inc., Waterford, NY, USA) at the concentration of 1% (according to Song' study [30]) were chosen as pesticide surrogates to compare their effects on initial atomization and spray drift, and pure water was the reference solution. It can be seen from Table 2 that the surface tension of silicone (21.377 mN/m) was the smallest.

Table 1. Parameters of the nozzles used in this experiment.

Nozzle	Nozzle Characteristics	Label Angle (°)	Applied Angle (°)	Manufacturer
XR	Flat fan	110	112	Teejet Technologies
AIXR	Air induction	110	95	Teejet Technologies
TXVK	Hollow cone	80	81	Teejet Technologies

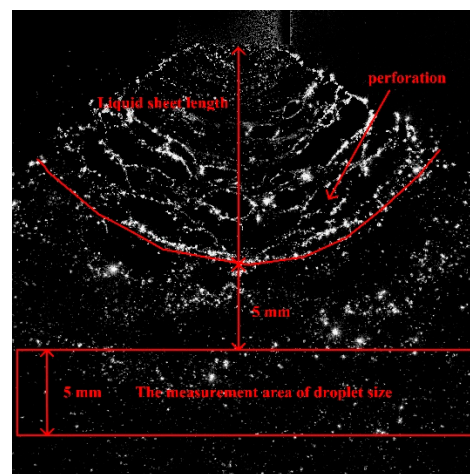
Table 2. Spray solutions mixed with different adjuvants.

Adjuvant	Volume Concentration (%)	Surface Tension (mN/m)	Manufacturer
Water	100	72.8 ± 0.021	Ultra-pure water, Medford, OR, USA
SDS	1	33.310 ± 0.092	neoFroxx GmbH
AOT	1	26.631 ± 0.267	Aladdin Biochemical Technology Co., Ltd.
Silicone	1	21.377 ± 0.064	Momentive Performance Materials Inc.

2.5. Data Analysis

To ensure the adequate breakup of the liquid sheet and obtain the information of initial droplets for the description of a wide variety of flow conditions, the droplet group in the spray belt with a thickness of 5 mm was intercepted from 5 mm below the breaking point of the liquid sheet (Figure 3), which was measured using Insight 4G software. The irregular droplet diameter was corrected by Equation (2). The shortest and longest lengths of the irregular droplets corresponded to d_1 and d_2 , respectively.

$$d = \sqrt{d_1 d_2} \quad (2)$$

**Figure 3.** The diagram of test methods for the liquid sheet length and droplet size.

The approach that contains one single mean diameter provides an inadequate description for either the global or the local character of a spray. The probability volume density function (PDF_v) of droplet size is defined in terms of the volume fraction of the volume of droplets in a specified droplet size range to the total volume of droplets detected. In addition, the quantity density distribution, $D_{V0.5}$, and %<150 μm were selected to interpret the data of the overall spray. $D_{V0.5}$ is the droplet diameter (μm) at which 50% of the spray volume contains droplets at the given size and below. The %<150 μm is the percentage of the spray volume containing droplets 150 μm in diameter (a common threshold used to define driftable fines) and below and provides a parameter of the relative drift potential of each treatment [12,31,32].

The coefficient of variation (CV) was selected as the index to evaluate the fluctuation of the liquid sheet length, which was calculated by Equation (3).

$$CV = \frac{SD}{\bar{X}}, \text{ with } SD = \sqrt{\frac{\sum_{i=1}^n (x_i - \bar{X})^2}{n-1}} \quad (3)$$

where SD is the standard deviation; \bar{X} is the average liquid sheet length; x_i is the liquid sheet length in each frame, mm; and n is the total number of frames.

The drift potential (DP) [33] of different spray solutions for the three nozzles at the 2 m position of lines was calculated according to Equation (5), which was expressed as a percentage of the amount of spray liquid remaining airborne to the liquid amount sprayed from the nozzle during the test run. The airborne drift amount (A_d) at 2 m downwind from nozzle was evaluated from all target lines using the Formula (4)

$$A_d = \sum_{i=1}^n \left(\frac{d_i + d_{i+1}}{2} \right) \left(\frac{s}{w} \right) \quad (4)$$

$$DP(\%) = \frac{A_d}{\beta_V} \times 100\% \quad (5)$$

where d_i and d_{i+1} are the amounts deposited on lines i and $i + 1$, μL ; n is the number of lines at 2 m downwind from the nozzle; s is the width between the sampling lines, m; w is the sampling line diameter, m; and β_V is the amount of spray liquid during the test run, μL .

The drift potentials in different horizontal areas were also calculated by Equations (4) and (5).

2.6. Statistical Analysis

One-way analysis of variance (ANOVA) was used for the comparison of the liquid sheet length, droplet diameter, and drift potential between different adjuvant solutions and water, where “*” represents $p \leq 0.05$, “**” represents $p \leq 0.01$, “***” represents $p \leq 0.001$, and “****” represents $p \leq 0.0001$. In this paper, the software GraphPad Prism 9 (GraphPad, San Diego, CA, USA) was utilized to explicitly determine these values. More precisely, the error bars in the data graphs were expressed by the standard deviation.

3. Results

3.1. Liquid Sheet Breakup and Initial Atomization Results

3.1.1. Breakup Mode

The liquid sheet breakup images for the XR, AIXR, and TXVK with the addition of water, silicone, SDS, and AOT are in Figures 4–6. The breakup modes, namely, the closed-rim mode, open-rim mode, rimless mode, wave or ligament mode, and fully developed mode, were classified by Bai [34]. The closed-rim mode generally occurred at low-velocity jets. A chain flow structure with closed rim was observed in which a sheet was initially formed that subsequently contracted into a cylindrical stream. The open-rim mode appeared after the closed-rim mode with the increase in jet velocity, where the sheet width enlarged and droplets were peeled off from the closed rim. For the rimless mode, parts of the sheet disintegrated periodically farther downstream. At higher Reynolds numbers, the aerodynamic wave became dominant, and the sheet broke up into ligaments, along with the peeling of droplets from the edge of the sheet, the so-called “wave or ligament mode”. The fully developed mode was observed when the jet velocity was very high. Violent turbulence and breakup occupied the whole sheet so that no clear breakup characteristics could be read from the images.

The jet velocity was the critical factor in the evolution of liquid sheet for the XR nozzle, with the primary breakup being the wave and ligament mode (at 0.3 Mpa). Waves were caused by the violent interactions of aerodynamic turbulence, and finally, the liquid sheet broke up by the increase in maximum growth rate and amplitude. The liquid sheet structure was affected by each spray solution: this was demonstrated by the SDS and AOT

spray solutions resulting in a larger liquid sheet area than the water and silicone spray solutions. Holes formed at the lower part of the sheet with the addition of SDS adjuvant and grew with time until the sheet breakup had fully occurred. No significant differences were found between the water and silicone spray solutions.

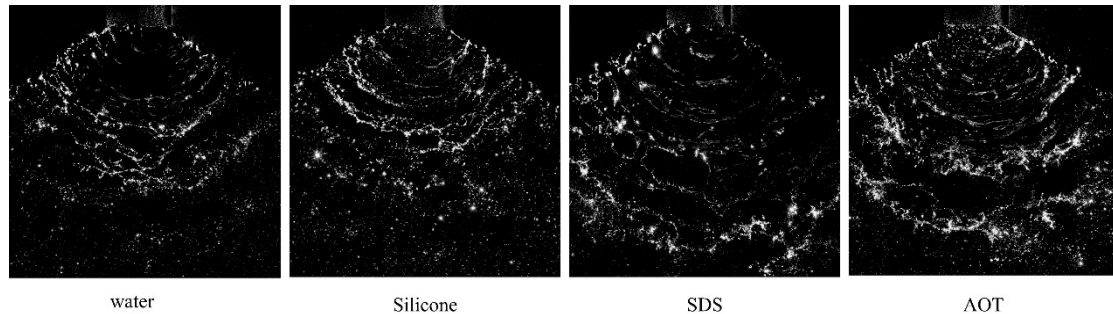


Figure 4. Spray images of XR nozzle with water, silicone, SDS, and AOT.

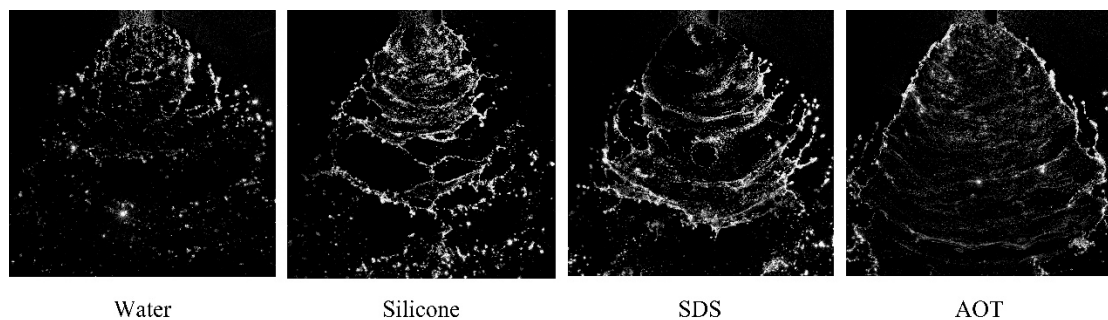


Figure 5. Spray images of AIXR nozzle with water, silicone, SDS, and AOT.

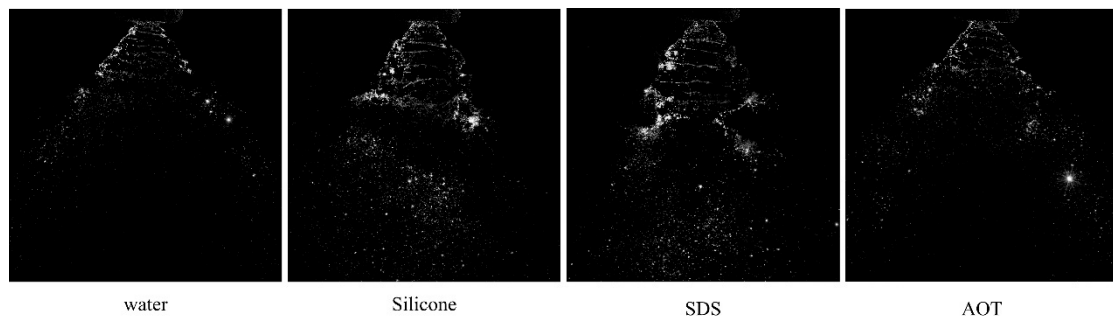


Figure 6. Spray images of TXVK nozzle with water, silicone, SDS, and AOT.

The AIXR nozzle entrained air within the sheet to alter the breakup pattern (and thus droplet size distribution) closer to the nozzle orifice. In comparison with spraying water, the addition of the adjuvant silicone, SDS, and AOT slightly extended the area of the liquid sheet, and the largest liquid sheet area was obtained by spraying AOT solution. When the silicone solution was sprayed, a web-like liquid sheet appeared, and then a large perforation was formed at the bottom part of the liquid sheet, followed by bow-like ligaments.

For the TXVK hollow cone nozzle, the mechanism of liquid sheet breakup was completely different from that of XR nozzle due to the difference in nozzle structure. Since the liquid was sprayed into the still air and then an internal suction flow was formed in the inner cavity of formed liquid sheet, it can be observed from Figure 6 that there were also droplets inside the liquid sheet cavity. The effects of the silicone and SDS spray solutions delayed the breakup of the liquid sheet (and thus the resulting droplet size distribution). The morphology and breakup distribution of the liquid sheet with the AOT solution was similar to that of water.

3.1.2. Liquid Sheet Length

Figure 7 illustrates the effects of the water, SDS, silicone, and AOT adjuvant solutions on the liquid sheet length for the XR, AIXR, and TXVK nozzles. In addition, the mean, standard derivation, CV values, and significance analysis of the liquid sheet length for the different treatments are calculated and shown in Table 3.

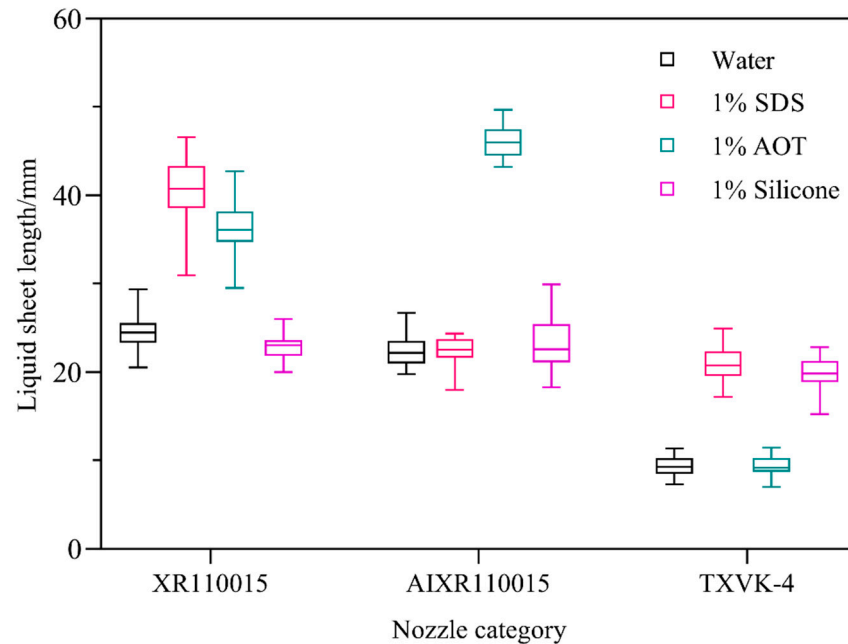


Figure 7. Liquid sheet length of four solutions for three kinds of nozzles.

Table 3. Mean, standard derivation, CV values, and significance analysis of the liquid sheet length for three types of nozzles under spray pressure of 0.3 Mpa.

Nozzle	Solution	Mean ¹ /mm	Standard Derivation	CV/%	p-Value ^{2,3}
XR110015	Water	24.49	1.84	7.50	0.000
	1% SDS	40.48	3.53	8.71	
	1% AOT	36.36	3.05	8.38	
	1% silicone	22.75	1.46	6.40	
AIXR110015	Water	22.39	1.77	7.89	0.822
	1% SDS	22.21	2.03	9.15	
	1% AOT	46.09	1.76	3.81	
	1% silicone	23.33	2.70	11.6	
TXVK-4	Water	9.28	1.06	11.4	0.000
	1% SDS	21.07	1.93	9.16	
	1% AOT	9.38	1.15	12.3	
	1% silicone	19.87	1.83	9.22	

Note: ¹ The mean of the liquid sheet length was calculated from 50 frames. ² Statistical significance was at $\alpha = 0.05$ with the LSD method. ³ The p-value was the significance between the water treatment and the adjuvant treatment.

The liquid sheet transients displayed dynamic periodic changes with time. The liquid sheet length changed compared with water for all nozzles since the adjuvants that determined the surface tension of the solution changed the physical properties of the spray solution (Figure 7).

ANOVA analysis was also employed for the liquid sheet length under different conditions. Water alone resulted in the shortest liquid sheet length, except for spraying the silicone solution with the XR nozzle and spraying the SDS solution with the AIXR nozzle. The liquid sheet lengths of the SDS (40.48 mm) and AOT (36.36 mm) solutions were

significantly longer than that of water alone (24.49 mm) at $p < 0.001$ for the XR nozzle, while the silicone (22.75 mm) solution was significantly lower than that of water alone at $p = 0.020$. For the AIXR nozzle, the liquid length of the AOT solution was significantly higher than that of water at $p < 0.001$. The average liquid sheet length of AOT (46.09 mm) solution was approximately two times higher than those of 1% SDS (22.21 mm), silicone (23.33 mm), and water (22.39 mm). For the TXVK nozzle, the high value ($p = 0.797$) of the AOT solution implied that there was no significant difference between the means of liquid sheet length for AOT and water, while the opposite results were obtained for the SDS and silicone solutions ($p < 0.001$). The breakup of the liquid sheet can lead to the generation of a large number of droplets. The droplet size, as an important attribute of droplets, may be affected by adjuvants and nozzle types.

3.1.3. Droplet Diameter

The droplet size characteristics following atomization are presented in Figures 8–10 and Table 4 in terms of probability volume density function (PDF_V), quantity density distribution, and droplet size parameters for the XR, AIXR, and TXVK nozzles with different solutions.

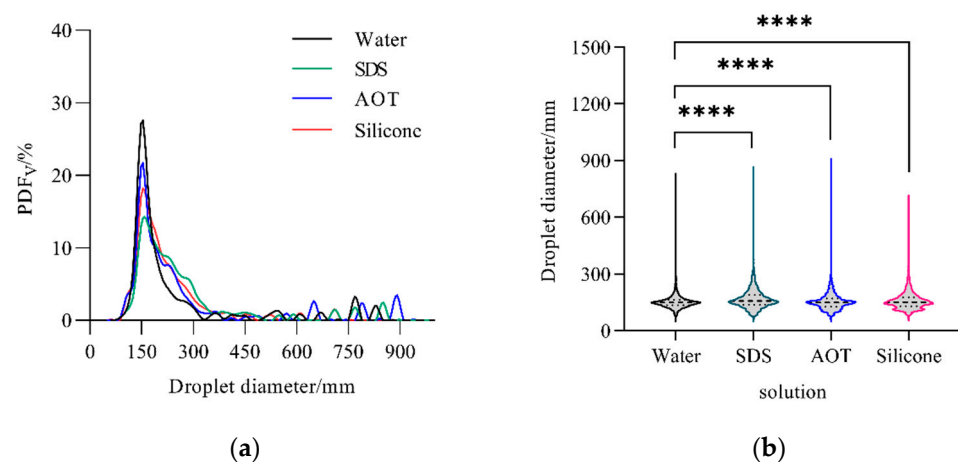


Figure 8. (a) Curve of probability volume density function (PDF_V). (b) Violin plots of drop size for the XR nozzle with different solutions. “****” indicates significance at $p \leq 0.0001$.

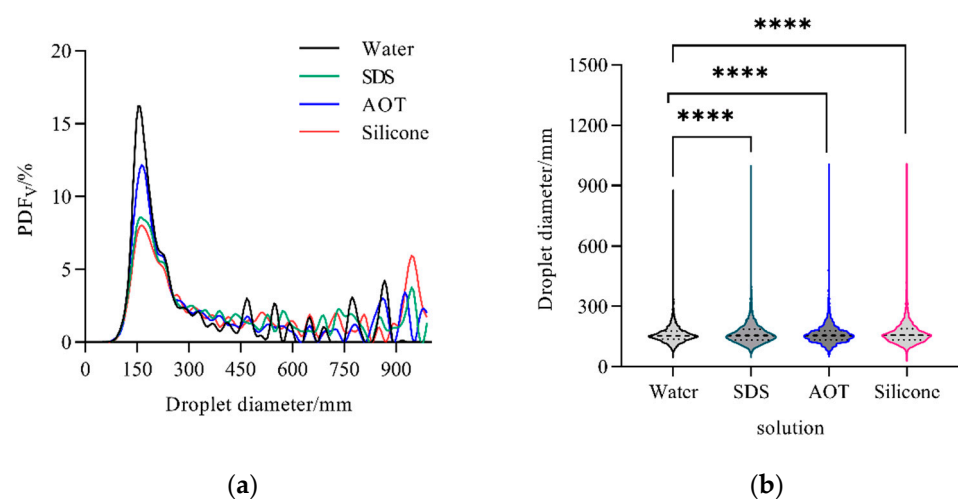


Figure 9. (a) Curve of probability volume density function (PDF_V). (b) Violin plot of drop size for the AIXR nozzle with different solutions. “****” indicates significance at $p \leq 0.0001$.

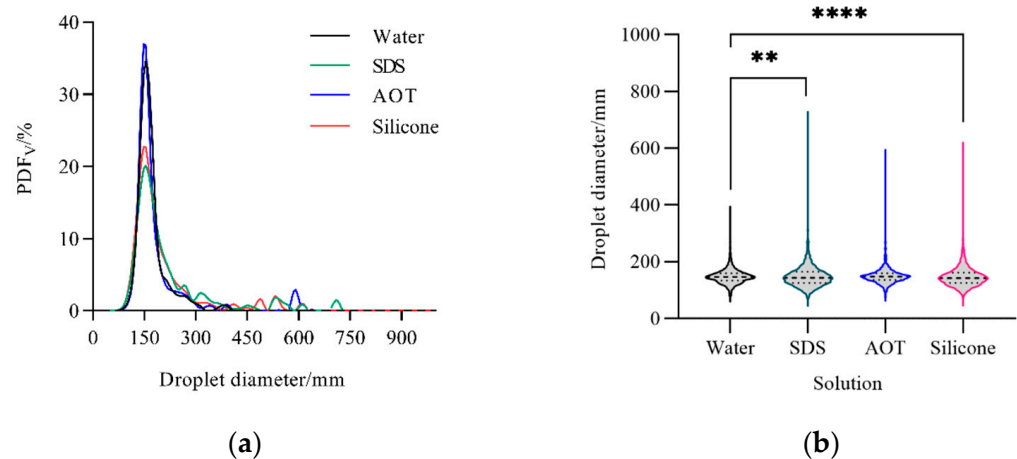


Figure 10. (a) Curve of probability volume density function (PDF_V). (b) Violin plot of drop size for the TXVK nozzle with different solutions. “***” and “****” indicates significance at $p \leq 0.01$ and $p \leq 0.0001$, respectively.

Table 4. D_{V0.5} and %<150 μm of the droplet size at different treatments.

	XR110015		AIXR110015		TXVK-4	
	D _{V0.5} /μm	<150 μm/%	D _{V0.5} /μm	<150 μm/%	D _{V0.5} /μm	<150 μm/%
Water	169	26.2	207	15.2	160	33.9
SDS	214	12.5	302	9.9	174	27.8
AOT	188	20.9	240	11.9	165	32.9
Silicone	190	19.4	328	8.7	167	32.0

As shown in Figures 8a, 9a and 10a, the peak of PDF_Vs curves all appeared in the droplet size range of 140–160 μm for all nozzles. The water alone resulted in the maximum peak compared with other solutions of the same nozzle except for the TXVK nozzle spraying AOT solution (Figure 10). Subsequently, the solutions in decreasing order of peak of PDF_V were the silicone and SDS treatments for both the XR and TXVK nozzles. For the AIXR nozzle, PDF_V at the peak displayed slightly larger values with the SDS solution (8.07%) than that with the silicone solution (7.38%), which was different from the results of the XR and TXVK nozzles. The reason for the difference in the PDF_V peak values across the four spray solutions could be due to the nozzle structure. Furthermore, the PDF_V distribution of droplets above 300 μm should be considered. Because the probability of drifting of large droplets is small, the method of increasing the droplet size is the major means of the anti-drift technology. The AIXR nozzle resulted in the highest PDF_V of droplets above 300 μm, and the TXVK nozzle resulted in the lowest PDF_V of droplets above 300 μm across all solutions.

In addition, comparisons of the overall spray droplet group within the analysis domain sprayed by the XR, AIXR, and TXVK across all solutions were made (Figures 8b, 9b and 10b). Overall speaking, water alone resulted in the most concentrated distribution in the droplet range of 140–180 μm for all treatments. The spray solution was significant for the size distribution of the droplet group at $p \leq 0.001$ for the XR and AIXR nozzles. The silicone and SDS solutions resulted in a significant difference in the size distribution of the droplet group compared with the water alone at $p \leq 0.001$ and $p = 0.0092$, while there was no significant difference between the AOT solution and water alone. The addition of adjuvant to water increases the proportion of larger droplets. Although it can be seen from Figures 8a, 9a and 10a that the addition of adjuvants changed slightly the size structure of the droplet group, the shape of the PDF_V curve changed greatly. This was due to the cubic relationship between the number and diameter of droplets in the case of constant spraying amount.

The $D_{V0.5}$ values with the adjuvant additions were 214 μm (SDS), 188 μm (AOT), and 190 μm (silicone), which were higher than that of water alone (169 μm) for the XR (Table 4). The $D_{V0.5}$ with silicone solution increased by 58.5% compared with water for the AIXR. The effect of adjuvant addition on the $D_{V0.5}$ was not obvious for the TXKV. In contrast, the characteristics of the percentage ($\%<150 \mu\text{m}$) used as a parameter to evaluate the drift probability of droplet groups were opposite to those of $D_{V0.5}$.

3.2. Wind Tunnel Experiments

3.2.1. Airborne Drift Potential

The measured drift deposition at the 2 m downwind position is shown in Figure 11. The error bars in the figure were determined by the standard deviation of the results of three repeated tests. Water alone resulted in the highest drift potential for the XR (6.95%), AIXR (2.47%), and TXVK (7.28%) nozzles compared with other solutions. This was not surprising given the droplet size results in Figures 8–10 and Table 4, where the adjuvant addition reduced the number of small droplets and increased the number of large droplets. The XR and TXVK were similar across four spray solutions, where the solutions in increasing order of drift potential were SDS, silicone, AOT, and water alone. The SDS adjuvant with the most effective drift reduction in XR and TXVK reduced the drift potential by 69.2% and 66.3%, respectively, while the silicone adjuvant with the largest drift reduction in AIXR reduced the drift potential by 78.3%. All adjuvants significantly reduced the drift potential for the XR, while the SDS solution sprayed by TXVK and no adjuvant solution sprayed by AIXR significantly reduced drift potential. The drift potentials were all lower obviously with the AIXR than those with the XR and TXVK nozzles across all solutions. On the whole, the TXVK nozzle has the highest drift potential under conditions of the same solutions compared with the other two nozzles.

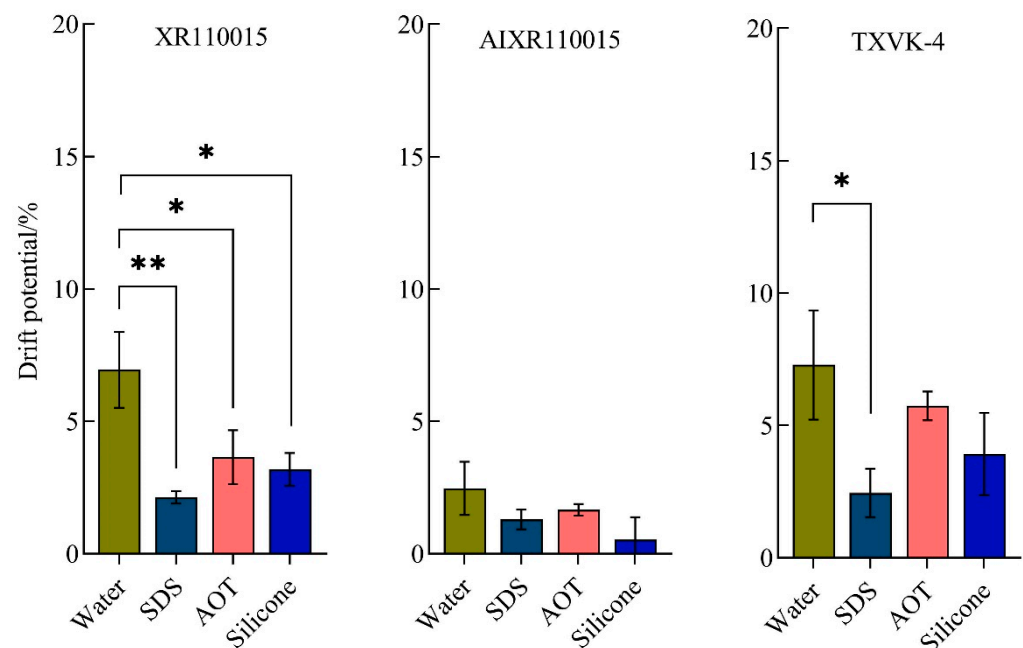


Figure 11. Drift potential percentages from polytetrafluoroethylene lines at the 2 m downwind position. “*” and “**” indicates significance at $p \leq 0.05$ and $p \leq 0.01$, respectively.

3.2.2. Drift Horizontally Downwind

The drift potential for all treatments is plotted in Figure 12. These data represent the average of the three repeated tests for each treatment. Overall, the variation in different treatments at various sampled distances was similar. The drift potential decreased as the downwind distance from the nozzle increased. The pure water yielded the highest drift potential at all drift distances (except the XR nozzle in the area from 8 m to 10 m) followed

by the AOT, silicone, and SDS solutions for the XR and TXVK nozzles, which was consistent with observations at the 2 m downwind location. The AIXR reduced significantly the drift potential at all drift distances compared with the XR and TXVK nozzles. Last, the highest drift potential occurred in the spray test of the TXVK nozzle. The drift potential in the area of 6 m to 7 m was roughly half of that in the area of 2 m to 3 m. The minimum drift potentials in the farthest area (from 9 m to 10 m) of the wind tunnel drift test area for XR, AIXR, and TXVK nozzle were 1.49%, 0.25%, and 1.27%, respectively.

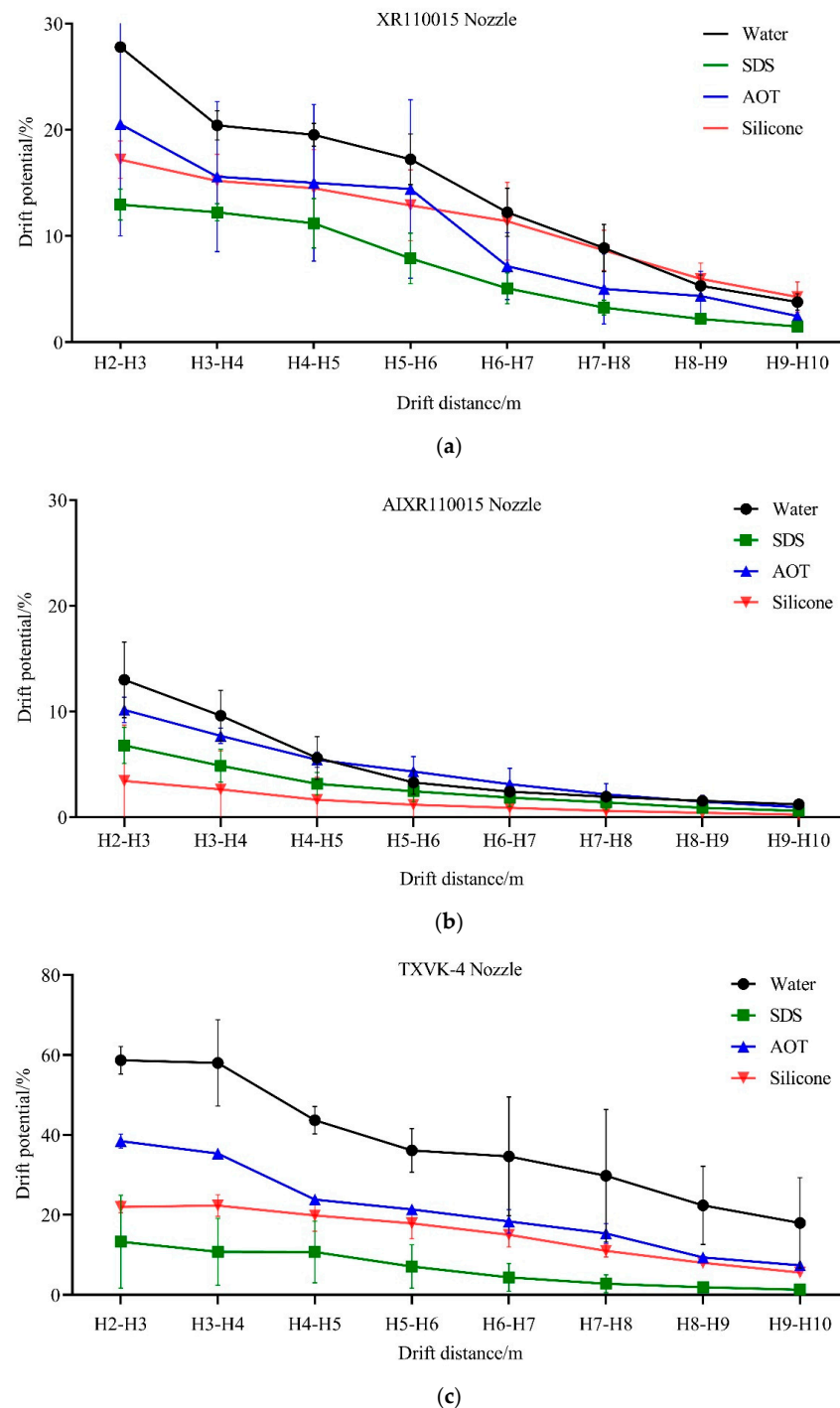


Figure 12. Drift potential curves in the area of 2 m to 10 m downwind for different spray solutions with the (a) XR, (b) AIXR, and (c) TXVK at a driving speed of 2 m/s. The abscissa represented the drift potential in the area between two adjacent sampling lines horizontally.

3.3. Correlation Analysis

A correlation analysis of the liquid sheet length and $D_{V0.5}$, the drift potential and $\%<150\ \mu\text{m}$, and the liquid sheet length and drift potential for the XR, AIXR, and TXVK nozzles was performed, as shown in Table 5. There were significant positive correlations between the drift potential and $\%<150\ \mu\text{m}$ for XR ($r = 0.921$), AIXR ($r = 0.974$), and TXVK ($r = 0.914$) nozzle. The liquid sheet length was positively correlated with the $D_{V0.5}$ for the XR ($r = 0.731$) and TXVK ($r = 0.833$) nozzles. Similarly, the liquid sheet length was negatively correlated with the drift potential for the XR ($r = -0.588$) and TXVK ($r = -0.932$) nozzles. For the AIXR nozzle, the correlations between the liquid sheet length and $D_{V0.5}$ and between the liquid sheet length and drift were weak, which was opposite to those of the XR and TXVK nozzles. This may be related to the complex process of liquid sheet breakup. When the liquid sheet length becomes longer, the thickness of the liquid sheet is thinner due to the principle of mass conservation. The thinner liquid sheet is more sensitive to aerodynamic disturbances and is prone to perforate the liquid sheet or break at the edge of the liquid sheet.

Table 5. Correlation coefficient of the liquid sheet length, $\%<150\ \mu\text{m}$, and the drift potential for the XR, AIXR, and TXVK-4 nozzles.

Item	XR110015	AIXR110015	TXVK-4
Liquid sheet length and $D_{V0.5}$	0.731	−0.329	0.833
Drift potential and $\%<150\ \mu\text{m}$	0.921 *	0.974 *	0.914 *
Liquid sheet length and drift potential	−0.588	0.111	−0.932

Note: “*” indicates statistical significance at $\alpha = 0.05$ level.

4. Discussion

Our results demonstrate the importance of adjuvant addition (AOT, SDS, and silicone adjuvant at the concentration of 1%) and nozzle type (XR, AIXR, and TXVK nozzle) on the liquid sheet breakup and the droplet size distribution in the analysis domain, as well as the drift potential at the 2 m downwind position and at different downwind distances. In this study, the liquid sheet breakup processes of all test nozzles were different across all spray solutions, and the breakup length of the liquid sheet and the droplet size distribution were significantly affected. Many studies have shown a close relationship between the droplet size spectrum and the drift at different positions downwind. Ferguson et al. [13] assessed the effect of application rates on the droplet size and drift potential, and the results represented that the drift potential was reduced by up to 85% when switching from a flat fan (TCP11002) nozzle spraying fine quality to an air induction (AIXR11002) nozzle spraying coarser spray quality. The droplet size at one or several points was an inadequate description of an entire spray, while the data were obtained from the entire spray area in this study using the PIV system. Moreover, the relationship between liquid sheet breakup and the size of the subsequently broken droplets [26], as well as the relationship between the droplet size and drift [35], have been proved by theoretical or experimental methods over the past 65 years. In the present study, the liquid sheet flow characteristics using different types of nozzles differentially influenced the liquid sheet breakup process and droplet formation and then changed the degree of drift. Due to diverse nozzle structures, the formed liquid sheet varied in shape. The volume median droplet sizes ($D_{V0.5}$) of water sprayed by the AIXR and TXVK nozzles increased by 22.5% and decreased by 5.3%, respectively, resulting in a decrease of 64.5% and an increase of 4.7% in the drift potential at the 2 m downwind position compared with the XR nozzle. A similar relationship existed between the atomization characteristics and drift for other adjuvant solutions sprayed by the three nozzles. In a word, the liquid sheet breakup and the formation of the initial droplets have a significant influence on drop size and drift.

In the experiment, the same adjuvant did not consistently affect the droplet size and liquid sheet length of different nozzles. This might due to the different mechanisms of liquid sheet breakup for the three types of nozzles. In contrast with the flat fan nozzle, the

air induction nozzle adopting the Venturi principle, allowing air bubbles to be carried inside the liquid sheet and droplets, produces larger droplets. As a result of this process, many new gas–liquid interfaces are formed, creating multidirectional and complex movements of adjuvant molecules toward the interfaces. The hollow conical nozzle formed thin liquid sheets, which are extremely sensitive to aerodynamic disturbance and are easily broken into small droplets. The atomization characteristics of this hollow conical nozzle require a very short response time for the adjuvant molecules to move toward the interface. In this study, the air induction nozzle (AIXR) produced larger droplets, and the hollow conical nozzle (TXVK) produced smaller droplets, which agreed with the above mechanism analysis of the liquid sheet breakup. In the spraying process, pesticide adjuvants can improve atomization properties, prevent evaporation, and enhance wetting and spreading on target leaves [36]. Depending on the agricultural activity, choosing the appropriate nozzles and suitable adjuvants to improve the operation effect is crucial.

The results of our surface tension test were not consistent with the changes of liquid sheet length and droplet size, as shown in our test results. The surface tension of the surfactant solution measured by a tensiometer does not necessarily determine the liquid sheet breakup, because the bulk solution is static when testing the surface tension. When it comes to spraying, due to the pressure of the orifice and the disturbance of the air, there is turbulence on the rapidly expanding liquid sheet. As a result, the mechanisms of the reduction of surface tension with time are more complicated than those measured by the tensiometer [37]. The moving liquid sheet may accelerate the reduction of surface tension due to the convection, or the mutual movement of liquid molecules may hinder the movement of surfactant molecules toward the interface [38]. In addition, the ability of adjuvants to move toward the interface is also different, which is independent of the equilibrium surface tension.

Spray solutions significantly affected the liquid sheet breakup, initial droplet diameter, and drift including the drift potential at the 2 m downwind position and at different distances. The adjuvant addition sprayed by the AIXR nozzle resulted in the clear difference in liquid sheet breakup, PDF_V curve, quantity density distribution, and D_{V0.5}. However, an interesting finding was the result of a difference in drift potential without a clear change. This is because the droplet generated by the air induction (AIXR) with a small proportion of <150 µm (15.2%) is larger than that of conventional nozzles. Consequently, adjuvants have a limited role when it comes to the droplet clusters composed of large droplets. There was a significant positive correlation between <150 µm and drift potential for all nozzles. However, the correlation between the liquid sheet length and D_{V0.5} was positive for the XR and TXVK nozzles. It can be seen from our data results that adjuvant addition can increase the liquid sheet length, and hydraulic pressure can also enhance the liquid sheet length. Either way, the increase in the liquid sheet length makes the liquid sheet thickness thinner due to the principle of mass conservation, which leads to the liquid sheet being more sensitive to aerodynamic disturbance. From our spraying images, the liquid sheet with long length formed perforations, which continued to merge and eventually fell off from the liquid sheet body. In addition, ligament breakup and droplet detachment are also the initial atomization methods. Therefore, the breakup mode of the liquid sheet is complex, and the relationship between the liquid sheet length and droplet size does not show a simple correlation. The diameter description of the global character of a spray provided several methods including probability volume density function curve (PDF_V), quantity density distribution, volume median droplet sizes (D_{V0.5}), and <150 µm in this study. There was a slight variation in D_{V0.5} between the XR (169 µm) and TXVK (160 µm) nozzles when spraying water alone, but the <150 µm of TXVK was 29.3% larger than that of XR nozzle; thus, TXVK's drift potential was 34.4% larger than XR's. The drift was weakly correlated with the volume median droplet sizes, while being strongly correlated with <150 µm. Consistent with previous studies, the drift was heavily influenced by the percentage of fine droplets, not D_{V0.5} in the spray.

5. Conclusions

Herein, the nozzle type (XR, TXVK, and AIXR) and the spray solution (water, SDS, AOT, and silicone) were used to study the breakup characteristics via PIV technology. The spray drift deposited on downwind ground and airborne lines were also measured in a wind tunnel. The nozzle type and the spray solution were found to significantly affect the liquid sheet breakup characteristics. Under identical test conditions, AIXR produced large droplets with a small proportion of easily drifting droplets, and TXVK with short liquid sheet length produced small droplets. All adjuvants, especially SDS and silicone, contributed to the formation of large droplets and the reduction ($<150\ \mu\text{m}$) of easily drifting droplets. At the same time, switching from a fine spray quality (TXVK) to a coarse spray quality (AIXR) can reduce the drift potential by as much as 66.1% and reduce the drift potential at all downwind distances. The use of the SDS adjuvant reduced the drift potential of XR by 69.2% and that of TXVK by 66.3%. With the silicone addition, the droplet size was changed most dramatically, and 78.3% of the drift potential of AIXR was reduced. There was a close relationship between the atomization characteristics and drift. The correlation between the liquid sheet length and $D_{V0.5}$ was positive for XR and TXVK nozzle, and there was a significant positive correlation between $<150\ \mu\text{m}$ and drift potential for all nozzles.

Author Contributions: Conceptualization, Y.L. and Q.L.; methodology, C.S. (Changfeng Shan); software, Q.L. and H.Z.; validation, Y.L.; and C.S. (Cancan Song); formal analysis, C.S. (Cancan Song); investigation, C.S. (Cancan Song); resources, Y.L.; data curation, Q.L.; writing—original draft preparation, Q.L.; writing—review and editing, Q.L.; visualization, H.Z.; supervision, Y.L.; project administration, Y.L.; funding acquisition, Y.L. All authors have read and agreed to the published version of the manuscript.

Funding: This research was funded by the Leading Talents of Top Talents Program for One Case One Discussion of Shandong Province.

Institutional Review Board Statement: Not applicable.

Data Availability Statement: The data presented in this study are available upon request from the corresponding author.

Conflicts of Interest: The authors declare no conflict of interest.

References

1. Lan, Y.; Chen, S. Current status and trends of plant protection UAV and its spraying technology in China. *Int. J. Precis. Agric. Aviat.* **2018**, *1*, 1–9. [\[CrossRef\]](#)
2. Lee, S.-J.; Mehler, L.; Beckman, J.; Diebolt-Brown, B.; Prado, J.; Lackovic, M.; Waltz, J.; Mulay, P.; Schwartz, A.; Mitchell, Y.; et al. Acute Pesticide Illnesses Associated with Off-Target Pesticide Drift from Agricultural Applications: 11 States, 1998–2006. *Environ. Health Perspect.* **2011**, *119*, 1162–1169. [\[CrossRef\]](#) [\[PubMed\]](#)
3. Mostafalou, S.; Abdollahi, M. Pesticides and human chronic diseases: Evidences, mechanisms, and perspectives. *Toxicol. Appl. Pharmacol.* **2013**, *268*, 157–177. [\[CrossRef\]](#) [\[PubMed\]](#)
4. Leslie, K.; Koger, S. Toxicants and Environmental Health: A Psychological Issue. *J. Stud. Res.* **2012**, *1*, 19–30. [\[CrossRef\]](#)
5. Samiee, F.; Samadi, M.T.; Bahrami, A.; Poorolajal, J.; Ghafouri-Khosrowshahi, A.; Leili, M. Risk assessment of imidacloprid and dichlorvos associated with dermal and inhalation exposure in cucumber greenhouse applicators: A cross-sectional study in Hamadan, Iran. *Int. J. Environ. Anal. Chem.* **2021**, 1–16. [\[CrossRef\]](#)
6. Ellis, M.B.; Alanis, R.; Lane, A.; Tuck, C.; Nuytens, D.; van de Zande, J. Wind tunnel measurements and model predictions for estimating spray drift reduction under field conditions. *Biosyst. Eng.* **2017**, *154*, 25–34. [\[CrossRef\]](#)
7. Epa, U. Worker protection standard application exclusion zone requirements. *US Environ. Prot. Agency.* **2016**.
8. EFSA Panel on Plant Protection Products and their Residues (PPR). Scientific Opinion on Preparation of a Guidance Document on Pesticide Exposure Assessment for Workers, Operators, Bystanders and Residents. *EFSA J.* **2010**, *8*, 1501. [\[CrossRef\]](#)
9. Hamey, P.; Byron, N.; Hanley, L.; Leslie, W.; Morgan, N.; de Backer, E.; Steurbaut, W.; de Backer, E.; Vergucht, S. Project to assess current approaches and knowledge with a view to develop a Guidance document for pesticide exposure assessment. *EFSA Support. Publ.* **2009**, *6*, 26E.

10. Chen, P.; Douzals, J.P.; Lan, Y.; Cotteux, E.; Delpuech, X.; Pouxviel, G.; Zhan, Y. Characteristics of unmanned aerial spraying systems and related spray drift: A review. *Front. Plant Sci.* **2022**, *13*, 870956. [\[CrossRef\]](#)
11. Wang, G.; Han, Y.; Li, X.; Andaloro, J.; Chen, P.; Hoffmann, W.C.; Han, X.; Chen, S.; Lan, Y. Field evaluation of spray drift and environmental impact using an agricultural unmanned aerial vehicle (UAV) sprayer. *Sci. Total. Environ.* **2020**, *737*, 139793. [\[CrossRef\]](#)
12. Bergeron, V. Designing intelligent fluids for controlling spray applications. *Comptes Rendus Phys.* **2003**, *4*, 211–219. [\[CrossRef\]](#)
13. Ferguson, J.C.; Chechetto, R.G.; O'Donnell, C.C.; Dorr, G.J.; Moore, J.H.; Baker, G.J.; Powis, K.J.; Hewitt, A.J. Determining the drift potential of Venturi nozzles compared with standard nozzles across three insecticide spray solutions in a wind tunnel. *Pest Manag. Sci.* **2016**, *72*, 1460–1466. [\[CrossRef\]](#) [\[PubMed\]](#)
14. De Schampheleire, M.; Nuyttens, D.; Baetens, K.; Cornelis, W.; Gabriels, D.; Spanoghe, P. Effects on pesticide spray drift of the physicochemical properties of the spray liquid. *Precis. Agric.* **2009**, *10*, 409–420. [\[CrossRef\]](#)
15. Liu, Q.; Chen, S.; Wang, G.; Lan, Y. Drift Evaluation of a Quadrotor Unmanned Aerial Vehicle (UAV) Sprayer: Effect of Liquid Pressure and Wind Speed on Drift Potential Based on Wind Tunnel Test. *Appl. Sci.* **2021**, *11*, 7258. [\[CrossRef\]](#)
16. Nuyttens, D.; Schampheleire, M.; Steurbaut, W.; Baetens, K.; Sonck, B. Experimental study of factors influencing the risk of drift from field sprayers, Part 1: Meteorological conditions. *Asp. Appl. Biol.* **2006**, *77*, 703958.
17. Gil, E.; Gallart, M.; Balsari, P.; Marucco, P.; Almajano, M.P.; Llop, J. Influence of wind velocity and wind direction on measurements of spray drift potential of boom sprayers using drift test bench. *Agric. For. Meteorol.* **2015**, *202*, 94–101. [\[CrossRef\]](#)
18. Huang, Y.; Zhan, W.; Fritz, B.; Thomson, S.; Fang, A. Analysis of Impact of Various Factors on Downwind Deposition Using a Simulation Method. *J. ASTM Int.* **2010**, *7*, 220–237. [\[CrossRef\]](#)
19. Songchao, Z.; Xinyu, X.; Weicai, Q.; Zhu, S.; Suming, D.; Lixin, Z. Simulation and experimental verification of aerial spraying drift on N-3 unmanned spraying helicopter. *Trans. Chin. Soc. Agric. Eng.* **2015**, *31*, 87–93. [\[CrossRef\]](#)
20. Junfeng, W.A.N.G.; Wenbin, X.U.; Jianlong, W.E.N.; Xiaoying, W.A.N.G.; Botao, L.U.O. Numerical Simulation on Gas-liquid Phase Flow of Large-scale Plant Protection Unmanned Aerial Vehicle Spraying. *Trans. Chin. Soc. Agric. Mach.* **2017**, *48*, 62–69. [\[CrossRef\]](#)
21. Hoffmann, W.C.; Fritz, B.K.; Lan, Y. Using laser diffraction to measure agricultural sprays: Common sources of error when making measurements. *Int. J. Precis. Agric. Aviat.* **2018**, *1*, 15–18. [\[CrossRef\]](#)
22. Wang, S.; He, X.; Song, J.; Zhang, L.; Gary, J.; Andreas, H. Measurement comparison and fitted distribution equation of droplet size for agricultural nozzles. *Trans. Chin. Soc. Agric. Eng.* **2014**, *30*, 34–42. [\[CrossRef\]](#)
23. Dorr, G.J.; Hewitt, A.J.; Adkins, S.W.; Hanan, J.; Zhang, H.; Noller, B. A comparison of initial spray characteristics produced by agricultural nozzles. *Crop. Prot.* **2013**, *53*, 109–117. [\[CrossRef\]](#)
24. Walklate, P.J.; Miller, P.C.H.; Gilbert, A.J. Drift classification of boom sprayers based on single nozzle measurements in a wind tunnel. *Asp. Appl. Biol.* **2000**, *57*, 49–56.
25. Negeed, E.-S.R.; Hidaka, S.; Kohno, M.; Takata, Y. Experimental and analytical investigation of liquid sheet breakup characteristics. *Int. J. Heat Fluid Flow* **2011**, *32*, 95–106. [\[CrossRef\]](#)
26. Zhang, J.; Liang, P.-F.; Luo, Y.; Guo, Y.; Liu, Y.-Z. Liquid Sheet Breakup Mode and Droplet Size of Free Opposed Impinging Jets by Particle Image Velocimetry. *Ind. Eng. Chem. Res.* **2020**, *59*, 11296–11307. [\[CrossRef\]](#)
27. Wei, Z.; Yongrui, H.; Xin, L.; Qi, L.; Xiaoming, F.; Bo, Z.; Haiyang, W.; Yingqian, W. Wind tunnel experimental study on droplet drift reduction by a conical electrostatic nozzle for pesticide spraying. *Int. J. Agric. Biol. Eng.* **2017**, *10*, 87–94. [\[CrossRef\]](#)
28. Torrent, X.; Gregorio, E.; Douzals, J.-P.; Tinet, C.; Rosell-Polo, J.R.; Planas, S. Assessment of spray drift potential reduction for hollow-cone nozzles: Part 1. Classification using indirect methods. *Sci. Total. Environ.* **2019**, *692*, 1322–1333. [\[CrossRef\]](#)
29. BS ISO 22856:2008; Equipment for Crop Protection—Method for The Laboratory Measurement of Spray Drift-Wind Tunnels. BSI Standards Limited: London, UK, 2008.
30. Song, M.; Ju, J.; Luo, S.; Han, Y.; Dong, Z.; Wang, Y.; Gu, Z.; Zhang, L.; Hao, R.; Jiang, L. Controlling liquid splash on superhydrophobic surfaces by a vesicle surfactant. *Sci. Adv.* **2017**, *3*, e1602188. [\[CrossRef\]](#)
31. Grover, R.; Kerr, L.A.; Maybank, J.; Yoshida, K. Field measurements of droplet drift from ground sprayers. *Can. J. Plant Sci.* **1978**, *58*, 611–622. [\[CrossRef\]](#)
32. Byass, J.B.; Lake, J.R. Spray drift from a tractor-powered field sprayer. *Pestic. Sci.* **1977**, *8*, 117–126. [\[CrossRef\]](#)
33. Nuyttens, D.; Taylor, W.; De Schampheleire, M.; Verboven, P.; Dekeyser, D. Influence of nozzle type and size on drift potential by means of different wind tunnel evaluation methods. *Biosyst. Eng.* **2009**, *103*, 271–280. [\[CrossRef\]](#)
34. Bai, F.; Diao, H.; Zhang, M.; Chang, Q.; Wang, E.; Du, Q. Breakup characteristics of power-law liquid sheets formed by two impinging jets. *Fluid Dyn. Res.* **2014**, *46*, 055506. [\[CrossRef\]](#)
35. Ru, Y.; Zhu, C.; Bao, R.; Li, Z.; Ding, T. Droplet size distribution of aerial nozzle for plant protection in wind tunnel and flight conditions. *Trans. Chin. Soc. Agric. Eng.* **2016**, *32*, 94–98. [\[CrossRef\]](#)
36. Wei, J.; Tang, Y.; Wang, M.; Hua, G.; Zhang, Y.; Peng, R. Wettability on plant leaf surfaces and its effect on pesticide efficiency. *Int. J. Precis. Agric. Aviat.* **2020**, *3*, 30–37. [\[CrossRef\]](#)

37. Ellis, M.B.; Tuck, C.; Miller, P. How surface tension of surfactant solutions influences the characteristics of sprays produced by hydraulic nozzles used for pesticide application. *Colloids Surf. A Physicochem. Eng. Asp.* **2001**, *180*, 267–276. [[CrossRef](#)]
38. Joos, P.; Petrov, P. The generalization of the Sutherland equation for continuously deforming surfaces. *Colloids Surf. A Physicochem. Eng. Asp.* **1998**, *143*, 273–282. [[CrossRef](#)]

Disclaimer/Publisher’s Note: The statements, opinions and data contained in all publications are solely those of the individual author(s) and contributor(s) and not of MDPI and/or the editor(s). MDPI and/or the editor(s) disclaim responsibility for any injury to people or property resulting from any ideas, methods, instructions or products referred to in the content.